WATER RESOURCES RESEARCH, VOL. 35, NO. 12, PAGES 3919–3929, DECEMBER 1999

Tidal networks
3. Landscape-forming discharges and studies in empirical geomorphic relationships

Andrea Rinaldo,[1] Sergio Fagherazzi,[2] Stefano Lanzoni, and Marco Marani
Dipartimento di Ingegneria Idraulica, Marittima e Geotecnica, Universitá di Padova, Padua, Italy

William E. Dietrich
Department of Geology and Geophysics, University of California, Berkeley

Abstract. In this final part of our study [*Fagherazzi et al*., this issue; *Rinaldo et al*., this issue] we propose a simple model for predicting the local peak ebb and flood discharges throughout a tidal network and use this model to investigate scaling relationships between channel morphology and discharge in the Venice Lagoon. The model assumes that the peak flows are driven by spring (astronomical) tidal fluctuations (rather than precipitation-induced runoff or seiche, sea surge, or storm-induced tidal currents) and exploits the procedure presented by *Fagherazzi et al*. [this issue] for delineating a time-invariant drainage area to any channel cross section. The discharge is estimated using the Fagherazzi et al. model to predict water surface topography, and hence flow directions throughout the channel network and across unchanneled regions, and the assumption of flow continuity. Water surface elevation adjustment, not assumed to be instantaneous throughout the network, is defined by a suitable solution of the flow equations where significant morphological information is used and is reduced to depending on just one parameter, the Chézy resistance coefficient. For the Venice Lagoon, peak discharges are well predicted by our model. We also document well-defined power law relationships between channel width and peak discharge, watershed area, and flow, whereas curved, nonscaling relationships were found for channel cross-sectional area as a function of peak discharge. Hence our model supports the use of a power law dependency of peak discharge with drainage area in the Venice Lagoon and provides a simple means to explore aspects of morphodynamic adjustments in tidal systems.

1. Introduction

In fluvial basins the key character of openness to mass/energy injection, central to their evolutionary dynamics, is usually enforced by assuming that total contributing area, say A, is proportional to landscape-forming discharges, say Q, that is, $Q \propto A^{\beta}$, with $\beta \leq 1$ [e.g., *Leopold et al*., 1984]. Substitution of drainage area for formative discharge in landscape evolution theories simplifies models without eliminating complex behavior that may be central to network evolution. In particular, this substitution permits effectively parameter-free models to be developed that can explore the tendency for networks to self-organize [*Rodriguez-Iturbe and Rinaldo*, 1997].

In tidal networks a simple assumption of proportionality of watershed area and landscape-forming discharges cannot generally be made [*Leopold et al*., 1984, 1993; *Myrick and Leopold*, 1963; *Friedrichs*, 1995]. Nonetheless, we have observed that important features of the tidal channel system, that is, the drainage density, network length, channel width, and channel initiation, vary with watershed area (albeit not as simple power functions) [*Fagherazzi et al*., this issue; *Rinaldo et al*., this issue]. This occurs despite the fact that flood flows are not simply dependent on marsh drainage area. In order to improve our understanding of these relationships, we need to develop a means of estimating an effective discharge throughout the channel network.

The basic relationship employed in the past for coupling hydrodynamic and morphodynamic processes is an empirical linkage of cross-sectional area of tidal channels (or tidal inlets), say Ω, with "spring" (i.e., maximum astronomical) tidal prism or "spring" peak discharge, say Q, that is,

$$\Omega \propto Q^{\alpha}, \tag{1}$$

where α is a scaling coefficient typically assumed to lie in the rather wide range 0.85–1.20 [e.g., *Langbein*, 1963; *Myrick and Leopold*, 1963; *Harleman*, 1966; *Jarrett*, 1976; *Nichols et al*., 1991]. However, the validity of (1) for sheltered channels (those not exposed to littoral transport or open sea) has recently been questioned [*Friedrichs*, 1995]. Complex and site-specific feedbacks between tidal channel morphology and tidal flow properties occur both in inlet and sheltered channel sections [e.g., *Bruun*, 1978; *O'Brien*, 1969; *Jarrett*, 1976; *Friedrichs*, 1995]. In addition, man-made interventions are key geomorphic agents in many lagoons; for example, artificial deepening of tidal channels, essential to navigability in many tidal environments exploited for port activity, may cause accelerated

[1]Also at Ralph M. Parsons Laboratory, Massachusetts Institute of Technology, Cambridge.
[2]Now at Computational Science and Engineering Program, Florida State University, Tallahassee.

Paper number 1999WR900238.
0043-1397/99/1999WR900238$09.00

deposition, as well as reductions of the tidal prisms by infilling or dyking marshes and/or lagoons. These modifications introduce time-dependent scales of influence on flow and erosion processes. Short-term, rapid, hydrodynamic adjustments of the order of days [*Byrne et al*., 1981] may occur. Longer-term adjustments due to subsidence and eustasy which affect the tidal prism propagation [e.g., *Gardner and Bohn*, 1980] may also be important. It seems also reasonable that morphodynamic relationships for channelized tidal embayments associated with the interior of tidal marshes or lagoons (or with the landward reaches of river estuaries opened to tidal fluctuations) work somewhat differently from inlets on open coasts. This stems, among other factors, from the relative lack of direct, intense wave attack and littoral drift in sheltered sites. Moreover, spatial gradients in tidal amplitude and phase are surely less pronounced than in the inlet zone.

In order to explore the applicability of (1) for sheltered tidal channels and to examine other morphologic relationships that could depend on discharge rather than just watershed area, we propose a hydrodynamic model that predicts the discharge throughout the network. This model allows us to examine the effects of differential flooding and draining of shallow unchanneled zones on peak discharges by exploiting the detailed topographic and morphological description of the tidal network. We first present the procedure for computing the discharge and then compare the scale of various morphological features with our computed peak discharges. We illustrate in detail the procedure for the computation of the landscape-forming flow rates and address the observational evidence of the morphological features (cross-section areas and widths and tidal basin watershed) with the maximum flow rates computed for each section. We also relate maximum flow rates to tidal prisms to check on their consistency. This leads us to some morphological remarks that close the paper.

2. Peak Spring Flow Rates at Arbitrary Cross Sections of a Tidal Embayment

Here we propose a simplified model for predicting the peak flow rates throughout the channel network of a tidal system which exploits our method [*Rinaldo et al*., this issue] for delineating the time-invariant watershed boundaries of individual subbasins. The model results can then be used to investigate possible relationships between channel morphology and discharge as has been done for entire tidal basins [e.g., *Marchi*, 1990].

Let x be the intrinsic, streamline coordinate defined by a tidal channel, assumed positive landward; let $\mathbf{x}$ be the arbitrary site within the tidal basin, that is, channelized or unchannelized; let t be the time coordinate; and let $V(t)$ be the instantaneous tidal volume stored within any arbitrary watershed which drains area A. Therefore, if $h(\mathbf{x}, t)$ is the free-surface elevation at time t (Figure 1) and $z(\mathbf{x})$ is the time-invariant bottom elevation, the instantaneous tidal volume is computed by

$$V(t) = \int_A [h(\mathbf{x}, t) - z(\mathbf{x})]\, d\mathbf{x}. \tag{2}$$

It is important to notice that A varies in time owing to the values of $h(\mathbf{x}, t)$. In fact, whenever $h(\mathbf{x}, t) < z(\mathbf{x})$ the bottom emerges, $h - z$ is set to zero, and the unit of area centered at

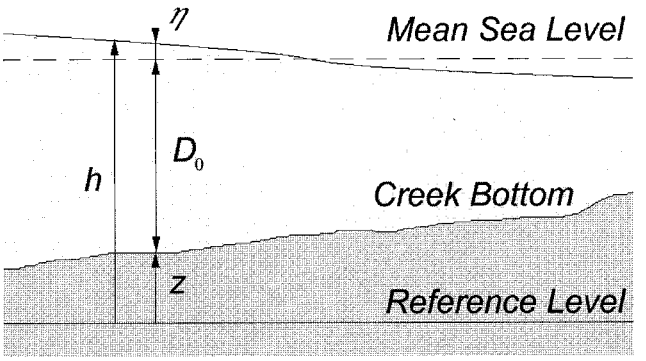

Figure 1. Notation used in the theory presented here: h is the height of water above the reference level, D_0 is the water depth with respect to the mean sea level (msl), η is water elevation above msl, and z is the bottom elevation with respect to the reference level.

$\mathbf{x}$ is removed from the watershed. This procedure yields what we term topographic nonlinearity.

In the above conditions, if U is the cross-section average of the flow velocity at an arbitrary outlet i (i.e., any location where all flows must pass through a cross section), where the morphological variables are the cross-section area Ω, width w, and depth $y = h - \bar{z}$ (in the last term the bar indicates a meaningful, cross-section-averaged, bottom elevation), then

$$\Omega U = \frac{dV}{dt} \tag{3}$$

(where discharge is obviously defined by $Q = \Omega U \sim wyU$), which is valid once the watershed is assumed time invariant. Equations (2) and (3) allow for the determination of $U_{\max}$ in flood and ebb and the values of $Q_{\max}$ whether or not maximum discharge coincides with times of maximum velocity (generally they do not [*Dronkers*, 1964; *Harleman*, 1966; *LeBlond*, 1978; *Pethick*, 1980; *Lanzoni and Seminara*, 1998a]). For estuarine tidal channels, *Myrick and Leopold* [1963] showed that the discharge occurring at the time of maximum velocity at a section is the pertinent leading flow rate. Field data [*Pethick*, 1980; *Healey et al*., 1981] show that in salt marsh creeks maximum velocities on the flood occur only after water spills onto the marsh surface, just before high water, while maximum ebbing velocities occur once the water has left the marsh surface and is flowing through the channel. Moreover, flood and ebb peak velocities increase with the amplitude of the overmarsh tide. Spring and storm tides therefore are likely to play the major role in shaping the channel geometry, the action of spring tides being more effective because of their regular fortnightly frequency.

The solution to the general problem (3) depends on the determination of tidal elevations $h(\mathbf{x}, t)$ for arbitrary sets of bottom geometries, z (possibly higher than h at times), and boundary conditions [e.g., *Dronkers*, 1964]. *Marchi* [1990] simplified the task by assuming that tidal variations dV can be computed by $dV = \nu A dh_2$, where A is the time-invariant watershed occupied regardless of elevation; h_2 is a reference tidal elevation computed by suitably accounting for energy dissipation and tidal lag, which are assumed constant for an entire embayment (i.e., the so-called "static" model). The reduction coefficient ν accounts for the instantaneous elevation differences arising within the tidal basin with respect to the

Table 1. Best Estimate of Tidal Harmonic Constants Used for the Prediction of Astronomical Tides in the Venice Lagoon

	M_2	S_2	N_2	K_2	K_1	O_1	P_1	S_1
Amplitude A, m	0.254	0.143	0.042	0.032	0.155	0.04	0.057	0.015
Phase ϕ, deg	120	324	343	117	82	256	97	262
Angular speed, deg/hr	28.9841	30.0	28.4397	30.0821	15.0411	13.9430	14.9589	15.0

Source is *Comune di Venezia* [1998].

reference value h_2 and thus allows us to define the true tidal prism only in an approximate manner. The approach is sound, as long as the validity of the so-called static assumption (i.e., where the fluctuations of tidal elevations are spatially uniform implying very short travel time of the tidal wave with respect to its period) is valid and provided no change in contributing area A occurs even when parts of the tidal basin become fully drained.

Consistent with our assumption underlying the method for watershed delineation [*Rinaldo et al*., this issue], we assume that flow directions are fixed (first) by the channel directions determined automatically in objective manner from digital terrain maps (DTMs) [*Fagherazzi et al*., this issue] within the channelized portion of the tidal basin and (second) by the gradients of the Poissonian potential surface [*Rinaldo et al*., this issue] for tidal expansion areas external to the channelized portion. While the first assumption seems quite reasonable in general, because the channel is in any case a fundamental attractor for the hydrodynamic flow directions, the second assumption, though critically simplifying the analytical treatment of the problem, is certainly less valid in general. Our assumptions in the watershed model of (third) small instantaneous spatial gradients of elevations (basically implying short embayments), (fourth) flat unchannelized areas and, (fifth) time invariance in watershed boundaries might result in somewhat poor estimation of flow direction in shallow areas. In well-developed network structures like those investigated in this paper [see, e.g., *Fagherazzi et al*., this issue, Figures 1–4], however, the variation in pathways across unchannelized areas is probably small, and watershed divide location may remain relatively fixed.

We also assume that landscape-forming events are due to spring peak discharges which are driven by astronomical conditions [*Boon*, 1975; *Friedrichs*, 1995]. These peak discharges, then, can be estimated by imposing as a boundary condition the appropriate astronomical tidal conditions. We can then use the approach similar to that of *Dronkers* [1972] to estimate tidal waves from the simple superposition of sinusoidal waves each characterized by a given amplitude and frequency.

The basic tidal constituents in the upper Adriatic Sea are eight (M_2, S_2, N_2, K_2, K_1, O_1, P_1, and S_1) [*Comune di Venezia*, 1998]. Thus the basic boundary condition at sea, $h_s(t)$, is given by

$$h_s(t) = h_0 + \sum_{i=1}^{M} a_i(\omega_i) \cos \omega_i t, \tag{4}$$

where h_0 indicates mean sea level (msl), $a_i(\omega_i)$ is the amplitude of the i component, and $\omega_i = 2\pi/T_i$, where T_i is the relevant astronomical period. Therefore, on setting $h_0 = 0$ m above msl, one gets $h_s(t) = \eta_s(t) = \Sigma_{i=1}^{M} a_i(\omega_i) \cos \omega_i t$, where $M = 8$ and the various values of ω_i and $a_i(\omega_i)$ are computed via published harmonic constants (for the Venice Lagoon, see *Comune di Venezia* [1998] and Table 1).

To solve (3), we first compute the tidal propagation up the channel network, where the deeper flows and the constrained flow directions (forced to follow the channel banks) permit a simple calculation. To do this, we neglect spatial gradients of fluid density (due, e.g., to salinity) and overall density currents assuming that they are negligible at times of landscape-forming flows.

Consistent with the approximate framework leading to watershed delineation, we will manipulate the flow equations to obtain closed-form solutions. If $h = z + D_0 + \eta$ is water surface elevation (here $z(\mathbf{x}) = z(x)$ is the bottom elevation, $D_0(\mathbf{x}) = D_0(x)$ is the depth with respect to a datum, that is, mean sea level, and $\eta(\mathbf{x}, t) = \eta(x, t)$ is the height of the tidal wave with respect to the mean water level, see Figure 1), the instantaneous discharge Q is defined as

$$Q = \Omega U = (D_0 + \eta) w U, \tag{5}$$

and, having set Coriolis' coefficient to zero [*Dronkers*, 1964], momentum and mass balance equations (neglecting wind effects which should not be meaningful in the average on astronomical flows) can be written as

$$\frac{\partial Q}{\partial t} - \frac{Q}{D_0 + \eta} \frac{\partial h}{\partial t} - \frac{Q}{w} \frac{\partial w}{\partial t} + \frac{Q}{\Omega} \left[\frac{\partial Q}{\partial x} - \frac{Q}{D_0 + \eta} \left(\frac{dD_0}{dx} + \frac{\partial \eta}{\partial x} \right) - \frac{Q}{w} \frac{\partial w}{\partial x} \right] = -g\Omega \left(\frac{dz}{dx} + \frac{dD_0}{dx} + \frac{\partial \eta}{\partial x} \right) - \frac{g}{\mathcal{C}^2 \Omega^2 (D_0 + \eta)} |Q| Q \tag{6}$$

$$\frac{\partial Q}{\partial x} + B \frac{\partial h}{\partial t} = 0 \tag{7}$$

where $\mathcal{C}$ is the Chézy coefficient, g is the acceleration of gravity, w is the channel width, and B is the width of channels plus adjacent storage regions, if any (all other symbols have been defined in the context of (3)).

The width B clearly depends on our watershed delineation procedure and can be computed, for each site, as follows. We compute watershed area A to a site characterized by a channel with width w; we move forward or backward by a small distance Δx (where w remains substantially unchanged) and measure the new watershed area $A + \Delta A$ and the channelized area $A' \sim w\Delta x$ occupied between the two stations. We then compute $B = \Delta A w / A'$ (Figure 2). This procedure allows for an adjustment of B at times when part of the tidal embayments is not underwater.

The continuity equation (7) uses the entire storage width (B) and accounts for changes in discharge per unit length due to over-bank flows by assuming that flow depth h is constant along B and changes instantaneously across the width. This assumption contributes to predict the experimentally observed reduction in tidal celerity through the main channels induced

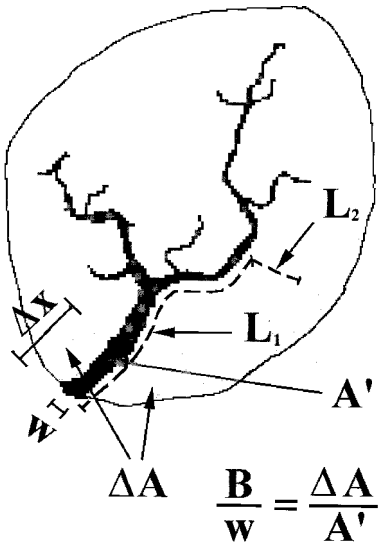

Figure 2. Geometrical relationships between changing storage on the plain and tidal wave propagation. Value w is the channel width, ΔA is the change of area along the channel distance Δx, A' is the area of the channel bed along Δx, and the travel distance to the outlet is composed of overland flow across the plain L_1 and the travel distance along the channel L_0. The effective cross-sectional width of the plain B is $\Delta A/\Delta x$, which is equivalent to $w\Delta A/A'$. The celerity c is thus corrected accordingly to account for the extent of adjacent storage zones. Notice that the watershed areas A, A' in two sections, and the width of the channel (all known from our geomorphic procedure) yield the collaborating width B.

by the expansion in adjacent storages [*Istituto di Idraulica dell'Universitá di Padova*, 1979].

In order to obtain a solution to the above equations, we make several important assumptions: (first) Spatial and temporal gradients of channel width w are negligible in the momentum equation; (second) flow velocities are smaller than a mean celerity of propagation of the tidal wave, that is, $U \ll \sqrt{g(D_0 + \eta)}$; and (third) in the main channels, tidal excursions are relatively small, that is, $\eta \ll D_0$. These assumptions are only valid for the larger tidal channels and for the lower tidal flats in mesotidal lagoons. In the smallest channels and along salt marshes these assumptions are seldom acceptable, and (8) will only yield a gross estimate of the local tidal flows.

To understand the impact of the proposed assumptions, a few observational figures from the Venice Lagoon case study may be significant. There the maximum value of η at the mouth for spring tides is $\eta \sim 0.30$ m which, in the experimental site where topography is accurately measured, is dissipated down to a few centimeters, typically 0.05–0.10 m. The depth D_0 of the channels ranges from $D_0 \sim 5$ m to less than 0.5 m, whereas tidal flats have, on average, depths from 0.5 to 1 m. The ratio η/D_0 thus ranges from less than 0.05 to 0.2 but may approach higher values for shallow salt marshes, and our assumptions are reasonable in most of the tidal embayment.

A further assumption we will employ is that energy losses can be linearized in the manner proposed by Lorentz [*Dronkers*, 1964; *Zimmermann*, 1982; *Jay*, 1991; *Friedrichs and Aubrey*, 1994] such that we can define a damping constant Λ as $\Lambda \sim gQ_m/\mathcal{C}^2\Omega_0 D_0$, where Q_m is the maximum value of Q, $\mathcal{C}$ is Chézy's coefficient, and Ω_0 is the cross-section area at datum elevation. Linearization of the frictional term is rigorously justified only in weakly dissipative tidal channels and is formally invalid in the case of strongly dissipative channels [*Lanzoni and Seminara*, 1998a]. Nevertheless, in strongly dissipative, weakly convergent, and relatively short channels as those typically observed in lagoons, a linearized approximation of frictional resistence still leads to acceptable results [*Friedrichs and Madsen*, 1992]. The relatively small distance the tidal wave travels, in fact, causes the distortion of the tidal wave enhanced by nonlinearities to be small.

Finally, following *Dronkers* [1964], we define for convenience two dimensionless parameters, $\sigma_i = [-1/2 + 1/2(1 + \Lambda^2/\omega_i^2)^{1/2}]^{1/2}$ and $\beta_i = [1/2 + 1/2(1 + \Lambda^2/\omega_i^2)^{1/2}]^{1/2}$, and assume the following boundary conditions: At $x = 0$, at the forcing tidal inlet, $h(0, t) = h_s(t)$; the other boundary condition, required by the second-order differential equation, varies depending on the problem at hand, and it could lead to resonant conditions. The general solution of (6) and (7) with the above stipulations is [*Dronkers*, 1964]

$$\eta(x, t) = \sum_{i=1}^{M} \left[\eta_{1i}(\omega_i) e^{\omega_i \sigma_i x/c_0} \cos \omega_i \left(t + \frac{\beta_i}{c_0} x \right) + \eta_{2i}(\omega_i) e^{-\omega_i \sigma_i x/c_0} \cos \omega \left(t - \frac{\beta_i}{c_0} x \right) \right] \quad (8)$$

$$c_0 = \sqrt{g \frac{\Omega_0}{w}} \sqrt{\frac{w}{B}}, \quad (9)$$

where the propagation velocity is represented by c_0/β_i. The boundary conditions determine η_{1i} and η_{2i} and must satisfy the requirement that M remains the same as that of the forcing modes because of the implied linearization, and $\eta_{1i}(\omega_i) + \eta_{2i}(\omega_i) = a_i(\omega_i)$. Clearly, many more harmonics are generated by topographic nonlinearities. The other boundary condition (i.e., at $x = \infty$ or imposing a reflecting barrier at some finite distance x_L) poses serious theoretical and practical problems [*Dronkers*, 1964]. In fact, a simple harmonic wave generated at $x = 0$ in a channel of infinite length would call for $\eta_{1i}(\omega_i) = 0$ thus considerably simplifying the analytical manipulations, while a finite length, say at $x = L$, requires the condition $Q(L, t) = 0$, which in some cases might induce resonance. Owing to the dissipative character of tidal networks and the fact that we are interested in a relatively accurate estimate of the decay and phase shift of tidal propagation, we will employ the infinite length approximation. Thus our estimate of the harmonic wave propagator within deeper channels is

$$\eta(x, t) \sim \sum_{i=1}^{M} a_i(\omega_i) e^{-\omega_i \sigma_i x/c_0} \cos \omega_i \left(t - \frac{\beta_i}{c_0} x \right). \quad (10)$$

The tidal propagation within the shallow storage zones adjacent to the channel requires a different model. Our time-invariant choice of watershed delineation defines average flow directions (i.e., time-averaged gradients of free surface elevations), and thus the flow equations can be reduced to intrinsic coordinates defined by the gradients of the free surface given by the Poissonian model described by *Rinaldo et al.* [this issue]. Therefore having chosen an arbitrary site $\mathbf{x}$ within the unchannelized basin, we can partition the total distance from $\mathbf{x}$ to the outlet $x = 0$ into two paths. The first, of length $L_1(\mathbf{x})$, is measured along the unchanneled basin from the site $\mathbf{x}$ to the

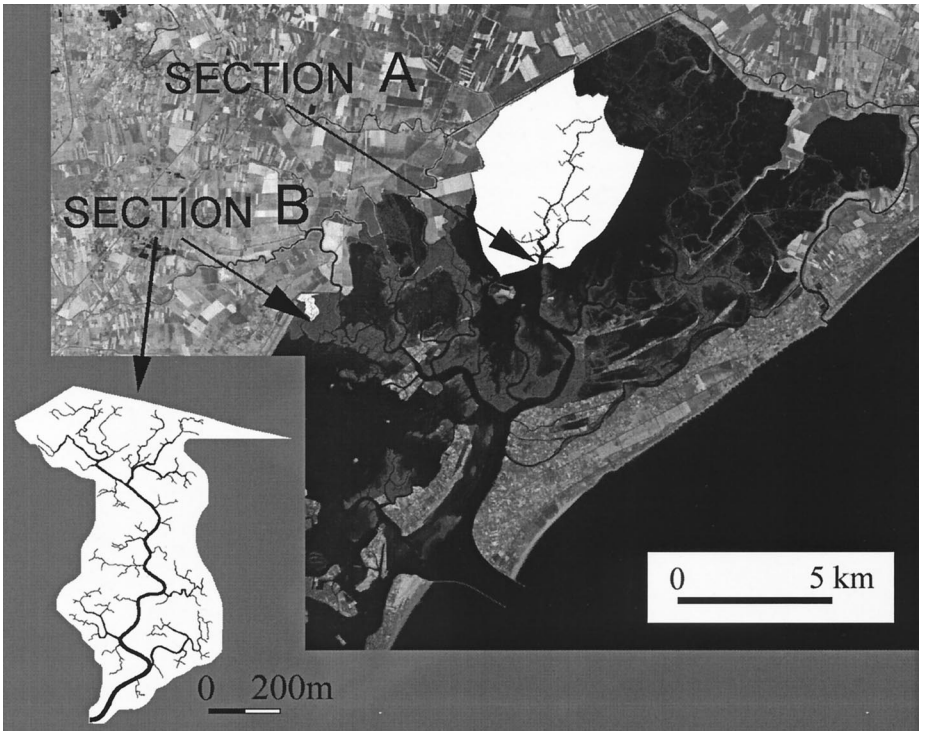

Figure 3. Location of the two tidal subbasins in the Venice Lagoon (Italy) where we apply our proposed procedure for predicting the spring peak discharges (which are driven by astronomical conditions). Basin A is larger, lies closer to the inlet, and has few channels, all favoring tidal conditions that prevent the emergence of the tidal flats at low tides. Section B lies in an area where tidal propagation uncovers large fractions of the watershed, enhancing nonlinear storage effects.

channel site with $x = L_0$ obtained at the intersection of the channel with the unique Poissonian streamline through **x** (thus defining a time-invariant outlet/inlet from and to the shallow storage zones). The second, of length L_0, is measured along stream from $x = L_0$ to the outlet ($x = 0$). Under our assumptions the basic mathematical form of the simple harmonic propagator is unchanged provided one accounts for the reduced tidal celerity, say $c_1 \sim \sqrt{gD_0(x)}$, which results from the smaller average flow depth $D_0(x)$ attained outside the channel network. The expression used to determine the delayed and damped oscillations at every site within a tidal basin then reads

$$\eta(\mathbf{x}, t) \sim \sum_{i=1}^{M} a_i(\omega_i) \exp\left[-\omega_i \left(\int_{L_0}^{L_0+L_1(\mathbf{x})} \frac{\sigma_{1i}}{c_1}\, dl + \int_0^{L_0} \frac{\sigma_{0i}}{c_0}\, dl \right) \right] \cdot \cos\, \omega_i \left(t - \int_{L_0}^{L_0+L_1(\mathbf{x})} \frac{\beta_{1i}}{c_1}\, dl - \int_0^{L_0} \frac{\beta_{0i}}{c_0}\, dl \right). \quad (11)$$

Notice that whenever $h < z$, one sets $D = 0$ and, accordingly, reduces the area used to compute the tidal storage volume in (2). This allows the computation of nonlinear topographic effects related to uncovering of storage zones characterized by shallow depths. The linear character of (11) does not allow generation of overtides or compound tides but, nevertheless, yields the asymmetries observed for bank-full tides. Topographic nonlinearities have been observed to critically affect stage-flow relationships in marsh creeks [e.g., *Pethick*, 1980; *Healey et al*., 1981]. We observe that asymmetries in ebb/flood discharges arise only whenever storage zones adjacent to the tidal network are placed at the critical elevation range affected by the oscillation of the water surface such that changes in the active watershed are pronounced.

3. Application of the Hydrodynamic Model to the Venice Lagoon

Figure 3 shows the test area chosen within the lagoon of Venice for application of the model. Here, for the sake of simplicity, we selected two cross sections draining tidal basins that differed in size, channel density, proximity to the tidal inlet, and vegetation. In the large basin (site A) we expect mostly linear response, whereas nonlinearities arising from complete drainage of the marsh plain (i.e., topographic nonlinearities) should be significant in the small basin (site B). Figure 4a illustrates the astronomical tide at the outer boundary of the lagoon of Venice, obtained by superposing the basic frequencies of Table 1. Figures 4b and 4c show plots of the forcing tide in the time window chosen for sections A and B, respectively; that is, they compare $\eta_s(t)$ and $\eta(x, t)$ via (11) for the two chosen sections A and B of Figure 3, windowed at the spring peaks producing the largest flow rates.

Notice that the only parameter required by the simulation of the tidal elevations via (11) is Chézy's coefficient, here assumed, for the sake of simplicity, to be spatially constant and equal to a standard value $\mathscr{C} = 40\ \mathrm{m}^{1/2}/\mathrm{s}$ both in channeled and unchanneled paths. Although it would be a simple task to assign a separate Chézy coefficient to the rougher shallow areas, we wanted to avoid any attempt here to fine tune this model, particularly since we are applying it to ungauged tidal

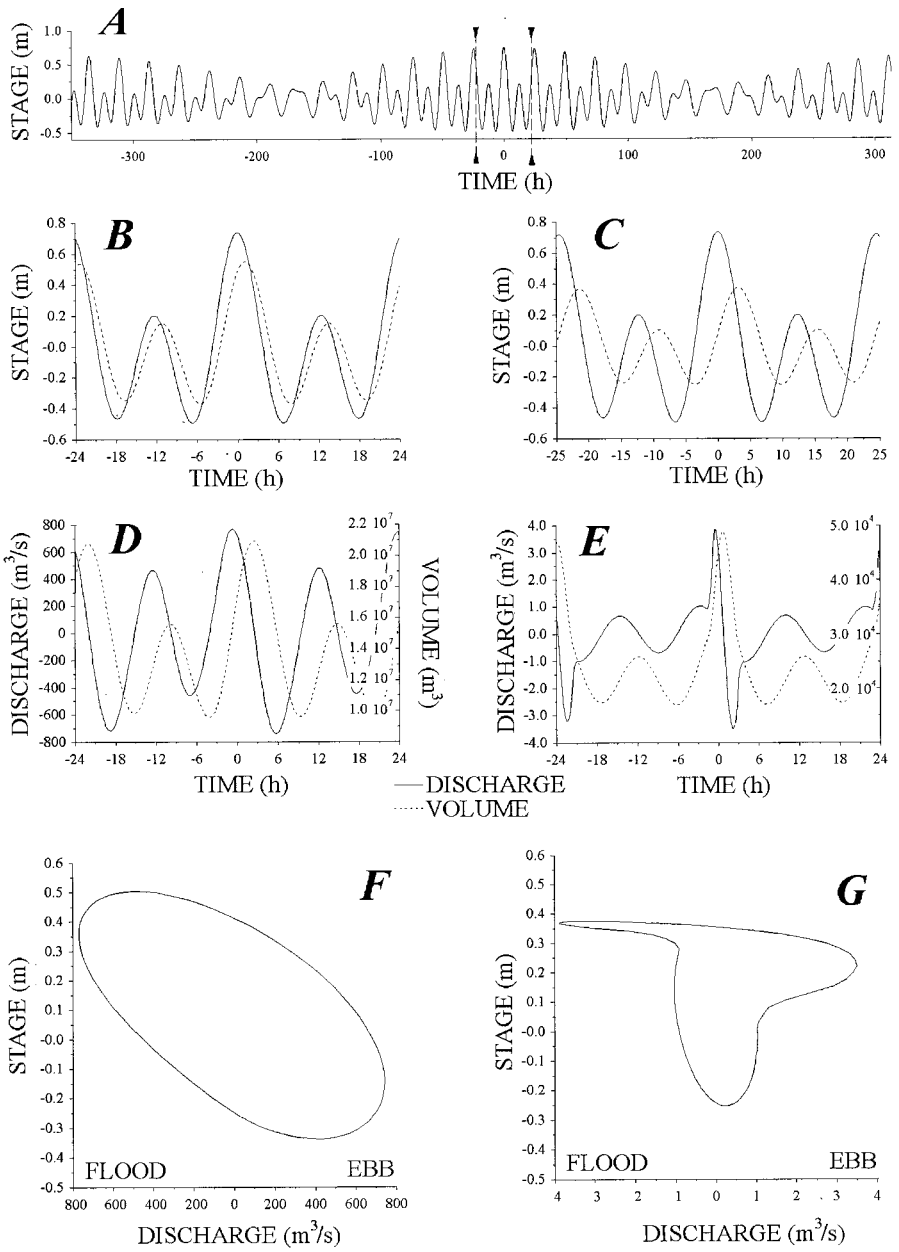

Figure 4. (a) Astronomical tides measured at the mouth of the Venice Lagoon, as produced by eight basic frequencies and the proper amplitudes. (b) A window of the astronomical tides within the lagoon. The solid line represents the tide at sea inlet, while the dotted line is the corresponding tide at section A of Figure 3, computed by equation (11) with a constant value of $\mathcal{C} = 40\ m^{1/2}/s$. (c) The same as in Figure 4b for section B of Figure 3. (d) Volume (solid line) and flow rates (dotted line) computed at section A. (e) The same as in Figure 4d for section B. (f) Stage-discharge relationship for section A during the tidal cycle of Figure 4b. (g) The same as in Figure 4f for section B.

basins in which details about the relative velocities in the channel and on the adjacent plain are not well documented.

In Figures 4d and 4e, volumes $V(t)$ and discharges $Q(t)$ are plotted against time for the two cross sections, A and B, respectively (Figure 3), by solving (2) and (3) owing to point-by-point knowledge of $h(\mathbf{x}, t)$ and $z(\mathbf{x})$ and suitable numerical quadrature.

Topographic nonlinear effects are evident when comparing the stage-discharge plots in Figures 4f and 4g. The smaller, more landward, and more channelized basin B experiences significant periods of complete marsh plain drainage, giving rise to the complex stage-discharge relationship in Figure 4g. This predicted behavior results from the influence of the threshold depth (i.e., when $h < z$ and $h - z = 0$). Qualitatively, the asymmetries induced in the stage-discharge relationship shown in Figure 4g conform with observational evidence [e.g., *Myrick and Leopold*, 1963; *Bayliss-Smith et al.*, 1978; *Healey et al.*, 1981; *French and Stoddard*, 1992]. In particular, for basins with marshlands that fully drain during a tidal cycle, the model predicts that the maximum flood discharge occurs just when the tide exceeds bank-full elevation and inundates the marsh surface. On the contrary, the maximum ebb discharge

occurs below bank-full elevation (a result similar to that reported by *Healey et al*. [1981] in their field study).

In order to further test the model, we have compared predicted and observed discharge at various sites in the Venice Lagoon. The *Istituto di Idraulica dell'Universitá di Padova* [1979] reported field measurements of discharge at several sites in the lagoon during a period of well-documented tidal forcing. The measured flow rates were forced by regular tides (thus not necessarily the ones producing the critical landscape-forming discharges). Only discharges within the channel were measured. To apply our model, we used the observed tidal cycle and assumed the Chézy coefficient $\mathcal{C} = 40\ \sqrt{\text{m}}/\text{s}$ throughout the system. Figure 5 shows the measured peak flow rates (both in flood and ebb) plotted against the predicted peak discharge for each site and the 1:1 line for perfect agreement. There may be a tendency to overpredict the discharge at low values and underpredict at the highest discharge. Despite the simplicity of the model, which only has one parameter (the Chézy coefficient), it predicts most of the values within 30%. This result justifies exploring how channel morphology varies with calculated peak discharges in the Venice Lagoon.

4. Morphologic Relationships to Peak Discharge

In order to explore the possible morphologic dependency on peak flows in the Venice Lagoon, we calculated the spring peak discharge using well established tidal data (Table 1). Figure 6 shows the relationship between Ω and the peak discharge $Q_{\max}$ for hundreds of sites along the tidal channel network of the northern lagoon of Venice. For channels with cross-sectional areas greater than about 50 m^2, a clear power law relationship emerges with an exponent close to 1.0; hence our model calculation agrees with (1) and the field observations reported by others elsewhere. The deviation at small cross-sectional areas occurs where there are progressively larger uncertainties in the analysis because of the small size of the channels. This is reflected in the progressive increase in the scatter of the data with smaller cross-sectional area (Figure 6). We interpret this apparent break in the power law relationship as being an artifact, then, of the poor morphologic resolution of small channels in our model. The corresponding, supposedly improved relationship including a measure of the hydraulic radius (here approximated by the mean depth of the cross sections $R \sim \bar{D}_0$, where the bar denotes cross-section average), that is, $\Omega R^{1/6}$ versus $Q_{\max}$ [*Friedrichs*, 1995], has also been studied. The deviation from the power law relationship still persists for small channels, and the overall pattern is very similar to that shown in Figure 6, and thus it has not been shown.

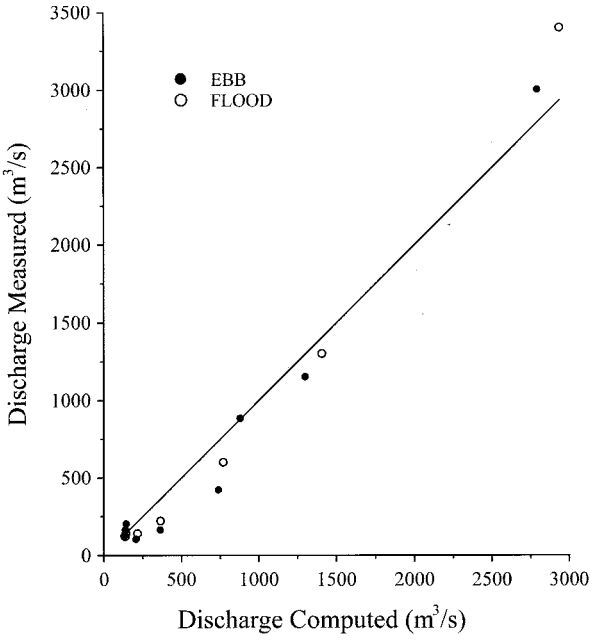

Figure 5. Measured discharge [*Istituto di Idraulica dell'Universitá di Padova*, 1979] versus computed discharge from the theory presented here for various sites in the Venice Lagoon.

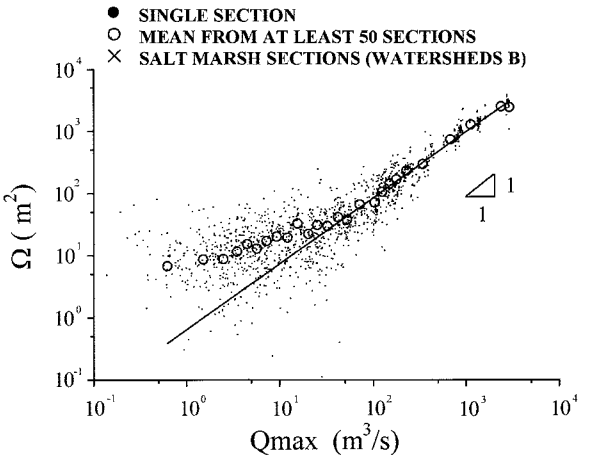

Figure 6. Cross-section area of tidal channels versus peak flow induced by astronomical tides. The dots represent the data from individual channel cross sections; the circles portray the ensemble mean (binned logarithmically [e.g., *Rodriguez-Iturbe and Rinaldo*, 1997, chapter 2]) of at least 50 cross sections. The solid line is the 1:1 slope. No major difference is noticeable if the cross-section area–peak flow relationship is corrected by the suggested 1/6 dependence on hydraulic radius [*Friedrichs*, 1995].

The approximate 1:1 relationship between cross-sectional area and stream power implies that the peak velocity is spatially constant. Figure 7 shows that while the calculated velocities for the larger channels are roughly constant, there is considerable variance for a given cross section. The boundary shear stress responsible for erosion and deposition is roughly proportional to the square of the velocity; hence this central tendency toward a spatially constant peak velocity may reflect an important morphologic adjustment toward a similar erosion potential. It may also then suggest that, as *Rinaldo et al*. [1995] have argued for fluvial systems, there is an important role of a threshold boundary shear stress in the network development.

Figure 8 shows that the relationship between peak discharge and channel width is a well-defined power law, with an exponent of 1.38, nearly identical to the power law relationship between drainage area and channel width reported by *Rinaldo et al*. [this issue]. Unlike fluvial systems the range in peak discharge increases to nearly 4 orders of magnitude for the smallest channel. Neglecting this variance and inverting the relationship of the means gives an exponent of w on discharge of 0.72. This value differs considerably from that reported for the small tidal basins documented by *Myrick and Leopold*

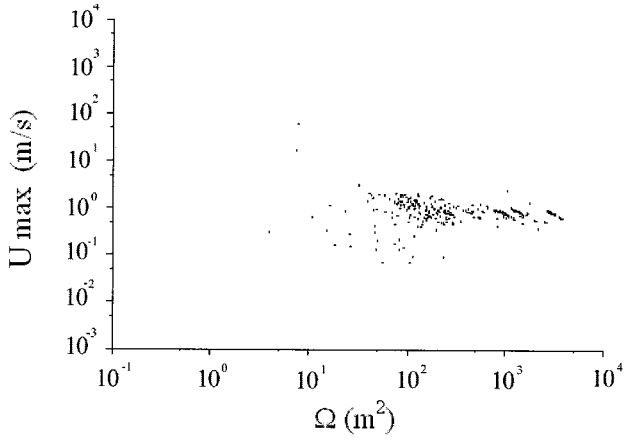

Figure 7. Maximum velocity generated by spring tides plotted versus the area of the cross section of the tidal channel where it is computed. Velocities are computed by dividing discharge (computed via equation (3)) by the actual cross-section area thereby fully accounting for propagation effects embedded in the evaluation of the instantaneous storage V.

[1963] (see also *Leopold et al*. [1984, 1993] in which the exponent is about 0.1. These empirical field studies relied on correlations with bank-full discharge, that is, the stage at which water begins to flow over the adjacent marshlands. Bank-full discharges and the maximum ebb or flood flow rates do not necessarily coincide in our scheme (see Figures 4f and 4g) and probably do not in nature.

The observation of the lack of a break in the relationship of peak flows and channel width (Figure 8) yields further interesting speculations. In fact, as shown in Figure 9, the corresponding relationship of cross-section area Ω with watershed area A, computed according to the procedure outlined by *Rinaldo et al*. [this issue], clearly shows a break analogous to that of Figure 6. We thus find that the factor showing a diverse behavior is undoubtedly the scaling of the mean depths h (across the cross section) with peak flows.

Two commonly used approximations in tidal networks are that the formative discharge varies with drainage area (although this is generally unlikely to be correct because of nonlinear effects) and that tidal prism surrogates peak discharge. Figure 10a shows that our model calculations for the northern Venice Lagoon predict that peak discharge is simply proportional to the upslope drainage area (shown in reverse for convenience in Figure 10a). Considerable scatter exists in the data, but, nonetheless, this simple result emerges. We do not know how general this might be, and on the basis of theoretical grounds we think it is not likely to be so. Figures 10b and 10c show the expected relationship between tidal prism (calculated either as the watershed area times the height of the tide at the outlet of the basin (Figure 10b) or from integration of (11) in time and space) and peak discharge. This supports the use of tidal prism as a measure of peak discharge.

5. Morphological Implications

The importance of asymmetric tidal cycles (i.e., the growth of compound constituents and harmonics in the tidal wave as it propagates through estuaries or lagoons) in the transport, accumulation, and/or erosion of sediment in shallow estuaries and coastal lagoons is well established [*Postma*, 1967; *Groen*, 1967; *Dronkers*, 1986; *Dyer*, 1973, 1986, 1995]. Moreover, the direction and intensity of the various sediment transport processes are related to size, shape, density, composition, and, to some degree, biological processing of sediment particles.

Coarser cohesionless fractions are usually transported as bed load in high-velocity channeled flow and often lead to the formation of estuarine dunes and bars [*Dalrymple and Rhodes*, 1995]. As observed by *Dronkers* [1986], bed load transport is mainly affected by the highest velocity and moves in the direction of the maximum current. In a tidal cycle with unequal duration and magnitude of ebb and flood the presence of a threshold for sediment movement and the strongly nonlinear character of the relationship between sediment transport rates and current velocity may cause significant asymmetry in sediment mobilization. In particular, a net landward sediment transport is induced in flood-dominated systems; conversely, in ebb-dominated systems a seaward directed transport is attained. The total load of suspended sediment, and its distribution within the water column over time, is also influenced by differences in flow acceleration during the two slack water

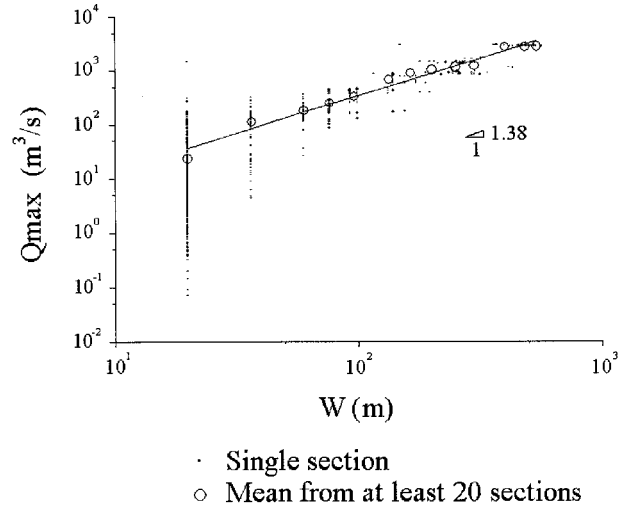

Figure 8. Plot of peak flow versus channel width, showing both individual points and ensemble averages (as described in the caption for Figure 6).

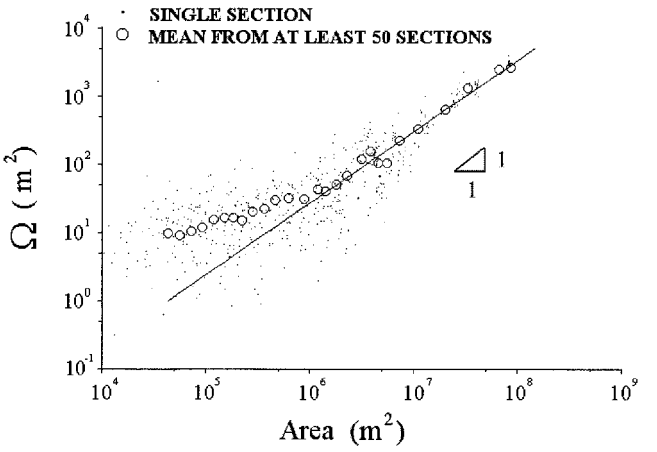

Figure 9. A plot of cross-section area Ω (m^2) versus watershed area A for the entire range of the Venice Lagoon. The symbols for single realizations and ensemble averages are as in the caption of Figure 6.

intervals. If the asymmetry between peak tidal velocities influences the amounts of eroded and resuspended sediments, the unequal duration of slack periods crucially affects sediment deposition. These effects, coupled with the phase lags between suspended sediment concentration and water velocity induced by the settling and erosion properties of mud, govern the continual and sometimes very rapid exchange between the suspension phase and the bed [*Kjerfve and Magill*, 1989; *Nichols and Boon*, 1994; *Dyer*, 1995].

In many estuaries the interplay of erosion and deposition may originate a broad zone of abnormally high suspended sediment concentration known as turbidity maximum. Although usually attributed to trapping of particles by the residual flow at the landward limit of salt penetration, the turbidity maximum may also have a tidal origin. The longer slack before ebb and the higher peak velocity during the flood typical of a flood-dominated system, in fact, favors the predominance of flood erosion and generates a net upstream transport. In the upper tidal reaches of the estuary, however, the tidal wave and currents progressively damp out, the flood dominance disappears, and net sediment transport is directed seaward by the flowing, river-like waters. A tidal sediment trapping zone (at times termed a "tidal node") is thus created at the upstream limit of tides, even in the absence of residual density circulation. Tidal nodes, however, are generally located farther upstream than the head of salt wedge intrusion [*Allen et al*., 1980]. Owing to the complex interplay of tidal transport and density circulation and to the periodical variations in mixing induced by the fortnightly spring-neap cycle or by the seasonal changes in freshwater discharge, the location of the tidal turbidity maximum is a transient feature, moving up and down an estuary or, presumably, a tidal network.

Within the lagoon interior the form of tidal asymmetry (and hence the net direction of sediment transport) depends on classifiable aspects of the general intertidal morphology. *Friedrichs and Aubrey* [1988] found that in well-mixed estuaries, nonlinear tidal distortion depends on (1) the frictional distortion in tidal channels (defined by the ratio a_0/D_0 of the tidal amplitude and the mean channel depth) and (2) the intertidal storage in tidal flats and salt marshes (defined by the ratio A_s/A_c of intertidal storage area occupied by tidal flats and marshes A_s and channel area covered by water at mean low tide A_c). Nonlinear friction results in greater frictional damping in shallow water, slowing the propagation around low tide. Thus the time delay between low water at the inlet and low water in the inner estuary is greater than the time delays between high waters, and flood dominates (this can be formally defined in terms of elevation and velocity phases [*Le Blond*, 1978; *Boon and Byrne*, 1981; *Speer and Aubrey*, 1985; *Friedrichs and Aubrey*, 1988, 1994; *Parker*, 1991; *Lanzoni and Seminara*, 1998a]). This behavior is enhanced by large values of the ratio a_0/D_0. Low velocities in intertidal marshes and flats also cause high tides to propagate slower than low tides. At low tide, in fact, marshes and flats are empty while channels are still relatively deep, allowing a faster exchange. Therefore the tidal wave is characterized by a relatively shorter ebb, longer flood, and highest velocity currents during the ebb (i.e., ebb dominance). Ebb dominance is thus favored by large A_s/A_c ratios.

The critical area of tidal flats needed to produce the transition from flood to ebb dominance has been discussed by *Friedrichs and Aubrey* [1988] and *Speer et al*. [1991]. Flood-dominant estuaries are typically shallow ($a_0/D_0 > 0.3$) with small to moderate areas of tidal flats. Ebb-dominated estuaries generally tend to be deeper ($a_0/D_0 < 0.2$) with frequently extensive regions of flats and marshes. *Boon and Byrne* [1981] suggested that flood-dominant tidal asymmetry can change to ebb-dominant asymmetry along with sedimentary infilling of a tidal basin. They argued that in a flood-dominant system without tidal flats, the landward directed sediment transport induced by tidal asymmetries may infill an initially deep basin, increase the area of flats, and eventually produce the transition to ebb dominance. *Friedrichs and Aubrey* [1988], however, noticed that an evolution from flood dominance to ebb dominance due to tidal asymmetry is possible only in weakly flood-dominated basins and would require sedimentary infilling which did not increase a_0/D_0, that is, formation of tidal flats and marshes at the edge of the tidal basin while maintaining

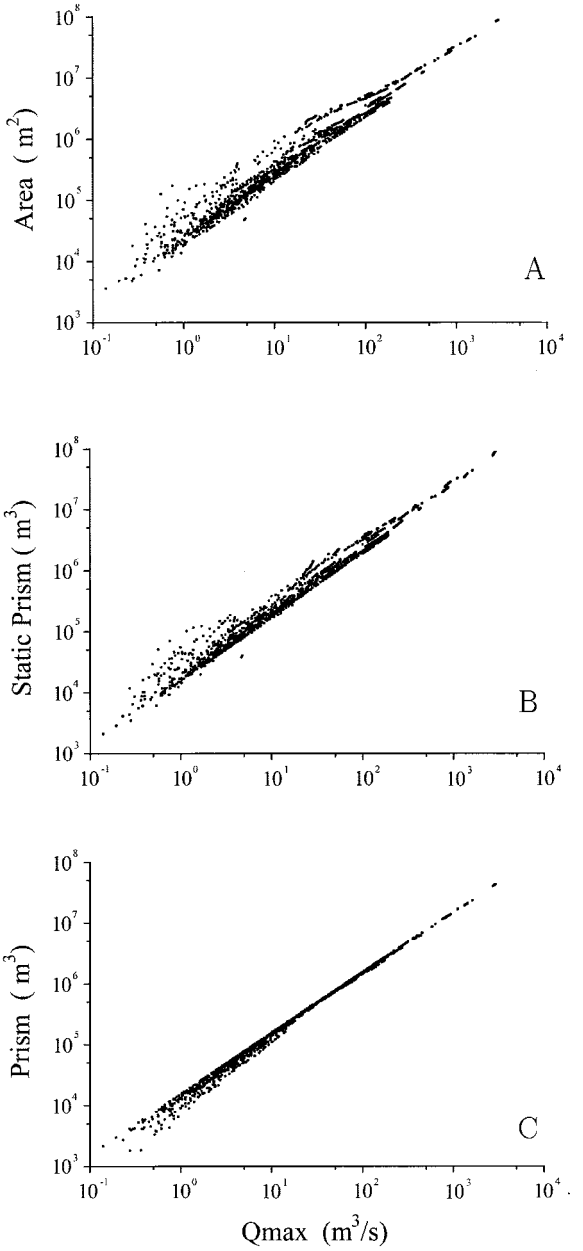

Figure 10. (a) Variation in watershed area. (b) Approximate tidal prism (watershed area A multiplied by tidal amplitude h at the watershed mouth). (c) Modeled tidal prism against peak discharge.

consistently deep channels. Whether or not this evolutionary pattern may actually occur is not clear.

In systems in which basin infilling is not advanced or where systematic dredging sustains D_0, there appears a tendency for flood dominance to occur particularly in landward shallower reaches of the creek network, while ebb-dominance may occur in the deepest parts of channel network [*Wright et al*., 1973]. Near inlet entrances, channel configuration and a_0/D_0 may discriminate flood or ebb dominance [*Dyer*, 1995] with flood tendency being enhanced by transport of wind-induced waves [*Boon and Byrne*, 1981]. So far, however, the question whether or not a transition between flood and ebb dominance may actually occur within coastal lagoons is not clearly understood nor documented.

Our data suggest that the possible signature of ebb/flood transition, as possibly marked by the break in Figure 6, may correspond to enhanced shoaling of the bed profile induced by the net landward transport of sediments produced by flood dominance. This fact would imply a break in the (cross-section average) longitudinal profiles of tidal channels of smaller, inner creeks. We notice that similar occurrences are observed in estuaries [e.g., *Collins et al*., 1986; *Speer et al*., 1991]. Moreover, a theoretical basis for the break in longitudinal profiles has been found from the study of shoaling phenomena at the critical point where the net sediment transport changes direction, that is, sea bound downstream and land bound upstream [*Lanzoni and Seminara*, 1998b]. This point could also mark the tidal turbidity maximum, although our results can merely suggest the validity of the above explanation.

6. Conclusions

We have proposed a procedure for determination of the maximum flow rates occurring at any arbitrary cross section in a tidal channel network. This procedure employs some ad hoc simplifications of the governing flow equations, which allows it to exploit our model [*Rinaldo et al*., this issue] for delineating marsh plain flow directions and local watershed areas. It is driven by a simple harmonic oscillator at the inlet which models observed tidal forcing, and it accounts for the effect of complete marsh surface drainage during the tidal cycle. This later effect creates what we have called topographic nonlinearity and produces a complex stage-discharge relationship where it is important. There is only one free parameter in the model, and that is the Chézy coefficient, which we have chosen to treat as spatially constant (i.e., the roughness difference between the marsh plain and the channel are not explicitly considered).

Despite its simplicity the model successfully predicts peak ebb and flood discharge for our northern Venice Lagoon study area. It gives well-defined power law relationships for larger channels between cross-sectional area, drainage area, tidal prism, channel width, and peak discharge. Variance, however, about the relationships is considerable, much larger than that reported for corresponding fluvial systems; nevertheless, the linkage of tidal hydrodynamics with the morphology of the tidal networks that we observe in nature holds in a surprisingly robust manner.

Acknowledgments. Funds provided by MURST (40%) National Project Morfodinamica fluviale e costiera and by the Università di Padova (1999/048/2/14/05/001) are gratefully acknowledged. The paper greatly benefited from a thorough review by Chris Paola and an anonymous reviewer and from discussions with Riccardo Rigon and Ignacio Rodriguez-Iturbe.

References

Allen, G. P., J. C. Salomon, P. Bassoullet, Y. Du Penhoat, and C. De Grandpré, Effects of tides on mixing and suspended sediment transport in macrotidal estuaries, *Sediment. Geol*., *26*, 69–90, 1980.

Bayliss-Smith, T. P., R. Healey, R. Lailey, T. Spencer, and D. R. Stoddart, Tidal flows in salt-marsh creeks, *Estuarine Coastal Mar. Sci*., *9*, 235–255, 1978.

Boon, J. D., Tidal discharge asymmetry in a salt marsh drainage system, *Limnol. Oceanogr*., *20*, 71–80, 1975.

Boon, J. D., and R. J. Byrne, On basin hypsometry and the morphodynamic response of coastal inlet systems, *Mar. Geol*., *40*, 27–48, 1981.

Bruun, P., *Stability of Tidal Inlets*, Elsevier, New York, 1978.

Byrne, R. J., R. A. Gammisch, and G. R. Thomas, Tidal prism-inlet area relations for small tidal inlets, *Proceedings of the 17th International Conference on Coastal Engineering*, pp. 2517–2533, Am. Soc. of Civ. Eng., Reston, Va., 1981.

Collins, L. M., J. M. Collins, and L. B. Leopold, Geomorphic processes of an estuarine marsh: Preliminary results and hypothesis, in *1986: Proceedings of the First International Conference on Geomorphology*, vol. 1, edited by V. Gardiner, pp. 1049–1071, John Wiley, New York, 1987.

Comune di Venezia and Istituto per lo Studio per la Dinamica delle Grandi Masse, Previsione delle altezze di marea per il bacino di S. Marco e delle velocitá di corrente per il Canal Porto di Lido–Laguna di Venezia: Valori astronomici, technical report, 33 pp., Ist. Poligr. dello Stato, Venice, Italy, 1998.

Dalrymple, R. W., and R. M. Rhodes, Estuarine dunes and bars, in *Geomorphology and Sedimentology of Estuaries*, *Dev. Sedimentol*., 53 pp., 1995.

Dronkers, J. J., *Tidal Computations in Rivers and Coastal Waters*, North-Holland, New York, 1964.

Dronkers, J. J., Des considérations sur la marée de la Lagune de Venise, *Atti Ist. Veneto Sci*., Lett. Arti, Commissione di studio dei provvedimenti per la conservazione e difesa della laguna e della cittá di Venezia, *5*, 81–106, 1972.

Dronkers, J., Tidal asymmetry and estuarine morphology, *Neth. J. Sea Res*., *20*, 117–131, 1986.

Dyer, K. R., *Estuaries: A Physical Introduction*, John Wiley, New York, 1973.

Dyer, K. R., *Coastal and Estuarine Sediment Dynamics*, John Wiley, New York, 1986.

Dyer, K. R., Sediment transport processes in Estuaries, in *Geomorphology and Sedimentology of Estuaries*, edited by G. M. E. Perillo, pp. 423–449, Elsevier, New York, 1995.

Fagherazzi, S., A. Bortoluzzi, W. E. Dietrich, A. Adami, S. Lanzoni, M. Marani, and A. Rinaldo, Tidal networks, 1, Automatic channel extraction and preliminary scaling features from digital terrain maps, *Water Resour. Res*., this issue.

French, J. R., and D. R. Stoddart, Hydrodynamics of salt marsh creek systems: Implications for marsh morphologic development and material exchange, *Earth Surf. Processes Landforms*, *17*, 235–252, 1992.

Friedrichs, C. T., Stability, shear stress and equilibrium cross-sectional geometry of sheltered tidal sections, *J. Coastal Res*., *11*(4), 1062–1074, 1995.

Friedrichs, C. T., and D. G. Aubrey, Nonlinear tidal distortion in shallow well-mixed estuaries: A synthesis, *Estuarine Coastal Shelf Sci*., *27*, 521–545, 1988.

Friedrichs, C. T., and D. G. Aubrey, Tidal propagation in strongly convergent channels, *J. Geophys. Res*., *99*, 3321–3336, 1994.

Friedrichs, C. T., and O. S. Madsen, Nonlinear diffusion of the tidal signal in frictionally dominated embayments, *J. Geophys. Res*., *97*, 5637–5650, 1992.

Gardner, C. R., and M. Bohn, Geomorphic and hydraulic evolution of tidal creeks on a subsiding beach ridge plain, North Inlet, S. C., *Mar. Geol*., *3–4*, 91–97, 1980.

Groen, P., On the residual transport of suspended matter by an alternating tidal current, *Neth. J. Sea Res*., *3*, 564–574, 1967.

Harleman, D. R. F., Tidal dynamics in estuaries, II, Real estuaries, in *Estuary and Coastal Hydrodynamics*, edited by A. T. Ippen, pp. 522–545, McGraw-Hill, New York, 1966.

Healey, R. G., K. Pye, D. R. Stoddart, and T. P. Bayliss-Smith, Velocity

variation in salt marsh creeks, Norfolk, England, *Estuarine Coastal Shelf Sci*., *13*, 535–545, 1981.

Istituto di Idraulica dell'Universitá di Padova, Le correnti di marea nella Laguna di Venezia, technical report, Minist. dei Lavori Pubbl., Comitato per lo studio dei provvedimenti a difesa della cittá di Venezia ed a salvaguardia dei suoi caratteri ambientali, (Studi e Richerche), 95 pp., Padua, Italy, 1979.

Jarrett, J. T., Tidal prism-inlet areas relationships, *GITI Rep. 3*, 136 pp., Coastal Eng. Res. Cent., U.S. Army Corps of Eng., Fort Belvoir, Va., 1976.

Jay, D. A., Green's law revisited: Tidal long-wave propagation in channels with strong topography, *J. Geophys. Res*., *96*, 20,585–20,598, 1991.

Kjerfve, B., and K. E. Magill, Geographic and hydrodynamic characteristics of shallow coastal lagoon, *Mar. Geol*., *88*, 187–199, 1989.

Langbein, W. B., The hydraulic geometry of a shallow estuary, *Int. Assoc. Sci. Hydrol*., *8*, 84–94, 1963.

Lanzoni, S., and G. Seminara, On tide propagation in convergent estuaries, *J. Geophys. Res*., *103*, 30,793–30,812, 1998a.

Lanzoni, S., and G. Seminara, Sull'equilibrio morfodinamico degli estuari, in *Proceedings of XXV Congresso di Idraulica e Costruzioni Idrauliche*, vol. 1, pp. 333–344, Coop. Univ. Editrice Catanese di Magistero, Catania, Italy, 1998b.

LeBlond, P. H., On tidal propagation in shallow rivers, *J. Geophys. Res*., *83*, 4717–4721, 1978.

Leopold, L. B., L. Collins, and M. Inbar, Channel and flow relationships in tidal salt marsh wetlands, *Tech. Rep. G830-06*, 78 pp., Calif. Water Resour. Cent., U.S. Geol. Surv., Univ. of Calif., Davis, 1984.

Leopold, L. B., J. N. Collins, and L. M. Collins, Hydrology of some tidal channels in estuarine marshlands near San Francisco, *Catena*, *20*, 469–493, 1993.

Marchi, E., Sulla stabilitá delle bocche lagunari a marea, *Rend. Fis. Mat. Accad. Lincei*, *9*, 137–150, 1990.

Myrick, R. M., and L. B. Leopold, Hydraulics geometry of a small tidal estuary, *U.S. Geol. Surv. Prof. Pap. 422-B*, 18 pp., 1963.

Nichols, M. N., and J. D. Boon, Sediment transport processes in costal lagoons, in *Coastal Lagoon Processes*, edited by B. Kjerfve, *Oceanogr. Ser*., vol. 60, pp. 157–211, Elsevier, New York, 1994.

Nichols, M. M., G. H. Johnson, and P. C. Peebles, Modern sediments and facies model for a microcoastal plain estuary, the James estuary, Virginia, *J. Sediment. Petrol*., *61*, 883–899, 1991.

O'Brien, M. P., Equilibrium flow areas of inlets in sandy coasts, *J. Waterw. Harbors Coastal Eng. Div. Am. Soc. Civ. Eng*., *95*, 2261–2280, 1969.

Parker, B. B., The relative importance of the various nonlinear mechanisms in a wide range of tidal interactions, in *Tidal Hydrodynamics*, edited by B. B. Parker, pp. 237–268, John Wiley, New York, 1991.

Pethick, J. S., Velocity surges and asymmetry in tidal channels, *Estuarine Coastal Mar. Sci*., *11*, 331–345, 1980.

Postma, H., Sediment transport and sedimentation in the estuarine environment, in *Estuaries*, edited by G. H. Lauff, pp. 158–179, Am. Assoc. for the Adv. of Sci., Washington, D. C., 1967.

Regione del Veneto, Carta tecnica regionale, map Venice, Italy, 1970.

Rinaldo, A., W. E. Dietrich, S. Vogel, R. Rigon, and I. Rodriguez-Iturbe, Geomorphic signatures of varying climate, *Nature*, *374*, 632–636, 1995.

Rinaldo, A., S. Fagherazzi, W. E. Dietrich, S. Lanzoni, and M. Marani, Tidal basins, 2, Watershed delineation and comparative network morphology, *Water Resour. Res*., this issue.

Rodriguez-Iturbe, I., and A. Rinaldo, *Fractal River Basins: Chance and Self-Organization*, Cambridge Univ. Press, New York, 1997.

Speer, P. E., and D. G. Aubrey, A study on non-linear tidal propagation in shallow inlet/estuarine systems, II, Theory, *Estuarine Coastal Shelf Sci*., *21*, 206–240, 1985.

Speer, P. E., D. G. Aubrey, and C. T. Friedrichs, Nonlinear hydrodynamics of shallow tidal inlet/bay systems, in *Tidal Hydrodynamics*, edited by B. B. Parker, pp. 321–339, John Wiley, New York, 1991.

Wright, L. D., J. M. Coleman, and B. G. Thom, Processes of channel development in a high-tide-range environment: Cambridge Gulf-Ord river delta, *J. Geol*., *81*, 15–41, 1973.

Zimmermann, J. T. F., On the Lorentz linearization of a quadratically damped forced oscillator, *Phys. Lett. A*, *89*(3), 123–124, 1982.

W. E. Dietrich, Department of Geology and Geophysics, University of California, Berkeley, Berkeley, CA 94720. (bill@geomorph.berkeley.edu)

S. Fagherazzi, Computational Science and Engineering Program, Florida State University, Tallahassee, FL 32306. (sergio@cse.fsu.edu)

S. Lanzoni, M. Marani, and A. Rinaldo, Dipartimento di Ingegneria Idraulica, Marittima e Geotecnia, Universitá di Padova, via Loredan 20, I-35131 Padua, Italy. (lanzo@idra.unipd.it; marani@idra.unipd.it; rinaldo@idra.unipd.it)

(Received August 5, 1998; revised July 16, 1999;
accepted July 21, 1999.)